Diverse ultrastructural landscape of atherosclerotic endothelium

Atherosclerosis 339 (2021) 35–45

Contents lists available at ScienceDirect

Atherosclerosis

journal homepage: www.elsevier.com/locate/atherosclerosis

Diverse ultrastructural landscape of atherosclerotic endothelium

Ewelina Kluza [a,b,*], Thijs J. Beldman [a], Annelie Shami [c], Edwin R. Scholl [d], Tsveta S. Malinova [e], Anita E. Grootemaat [d], Nicole N. van der Wel [d], Isabel Gonçalves [c,f], Stephan Huveneers [e], Willem J.M. Mulder [a,b,g,h,i], Esther Lutgens [a,j,k]

[a] Experimental Vascular Biology, Department of Medical Biochemistry, Amsterdam University Medical Center, Amsterdam, 1105, AZ, the Netherlands
[b] Laboratory of Chemical Biology, Department of Biomedical Engineering and Institute for Complex Molecular Systems, Eindhoven University of Technology, Eindhoven, the Netherlands
[c] Department of Clinical Sciences Malmö, Lund University, Clinical Research Center, Malmö, Sweden
[d] Electron Microscopy Center Amsterdam, Department of Medical Biology, Amsterdam University Medical Center, Amsterdam, 1105, AZ, the Netherlands
[e] Vascular Microenvironment and Integrity, Department of Medical Biochemistry, Amsterdam University Medical Center, Amsterdam, 1105, AZ, the Netherlands
[f] Department of Cardiology, Skåne University Hospital, Lund University, Sweden
[g] Biomedical Engineering and Imaging Institute, Icahn School of Medicine at Mount Sinai, New York, NY, 10029, USA
[h] Department of Oncological Sciences, Icahn School of Medicine at Mount Sinai, New York, NY, 10029, USA
[i] Department of Internal Medicine and Radboud Institute for Molecular Life Sciences, Radboud University Medical Center, Nijmegen, the Netherlands
[j] Institute for Cardiovascular Prevention, Ludwig Maximilians University, Munich, 80336, Germany
[k] German Center for Cardiovascular Research (DZHK), Partner Site Munich Heart Alliance, Munich, Germany

ARTICLE INFO

Keywords:
Atherosclerosis
Endothelium
Scanning electron microscopy
Endothelial junctions
Endothelial permeability

ABSTRACT

Background and aims: The endothelium plays a major role in atherosclerosis, yet the endothelial plaque surface is a largely uncharted territory. Here we hypothesize that atherosclerosis-driven remodeling of the endothelium is a dynamic process, involving both damaging and regenerative mechanisms.

Methods: Using scanning electron microscopy (SEM) and immuno-SEM, we studied endothelial junction ultrastructure, endothelial openings and immune cell-endothelium interactions in eight *apoe*$^{-/-}$ mice and two human carotid plaques.

Results: The surface of early mouse plaques (n = 11) displayed a broad range of morphological alterations, including junctional disruptions and large transcellular endothelial pores with the average diameter between 0.6 and 3 μm. The shoulder region of advanced atherosclerotic lesions (n = 7) had a more aggravated morphology with 8 μm-size paracellular openings at two-fold higher density. In contrast, the central apical surface of advanced plaques, *i.e.*, the plaque body (n = 7), displayed endothelial normalization, as shown by a significantly higher frequency of intact endothelial junctions and a lower incidence of paracellular pores. This normalized endothelial phenotype correlated with low immune cell density (only 5 cells/mm^2).

The human carotid plaque surface (n = 2) displayed both well-organized and disrupted endothelium with similar features as described above. In addition, they were accompanied by extensive thrombotic areas.

Conclusions: Our study unveils the spectrum of endothelial abnormalities associated with the development of atherosclerosis. These were highly abundant in early lesions and in the shoulder region of advanced plaques, while normalized at the advanced plaque's body. Similar endothelial features were observed in human atherosclerotic plaques, underlining the versatility of endothelial transformations in atherosclerosis.

1. Introduction

The arterial endothelium is a key player in atherogenesis and an integral cellular component of the atherosclerotic plaque [1,2]. Paradoxically, the endothelial plaque surface is largely unexplored. Our current knowledge is derived from fragmentary information provided by histopathology and, indirectly, from functional readouts including vessel wall permeability [3] and vascular tone [4]. The understanding of atherosclerosis-associated endothelial remodeling processes has a high clinical relevance since, next to the plaque rupture, surface damage, *i.e.*,

* Corresponding author. Groene Loper 2, 5612, AZ, Eindhoven, the Netherlands.
E-mail address: e.kluza@tue.nl (E. Kluza).

https://doi.org/10.1016/j.atherosclerosis.2021.11.017
Received 25 July 2021; Received in revised form 15 November 2021; Accepted 16 November 2021
Available online 19 November 2021

'plaque erosion', has been identified as one of the leading causes of thrombus formation and acute cardiovascular events [5–7]. At present, however, we lack a clear definition of endothelial damage and mechanistic insights into this process.

In general, the atherosclerotic plaque surface is considered an abnormal endothelial layer and a site of immune cell adhesion and transmigration [8,9]. Non-invasive functional imaging has shown enhanced permeability of the atherosclerotic vessel wall, indicative of a disturbed endothelial barrier [10,11]. However, many studies have linked this phenomenon to the neovasculature in plaque and/or adventitia rather than to the abnormalities of the primary vascular endothelium [12]. Similarly, different vascular pathways and transendothelial mechanisms of leukocyte recruitment to the lesion site are considered [13,14]. Consequently, an all-encompassing view on atherosclerotic plaque endothelium and its involvement in disease progression is still evolving.

Endothelial barrier integrity is regulated by the adherens junction proteins and their interactions with the cytoskeleton [15]. Vascular endothelial cadherin (VE-cadherin) is a key player in this protein complex, supported by intracellular catenins that are anchored to actin filaments [16]. Under physiological conditions, VE-cadherin is organized into continuous endothelial cell-cell junctions, whereas, upon inflammatory stimulation, VE-cadherin junctions undergo spatial reorganization into focal perpendicularly oriented clusters [17,18]. The latter phenotype has been associated with the loss of endothelial barrier integrity *in vitro*. However, both the *in vivo* occurrence and ultrastructural morphology of these remodeling junctions remain to be explored.

Previously, we have investigated the arterial endothelial structure and function in mouse atherosclerotic lesions [19]. By applying *en face* fluorescence microscopy, we found a significantly lower continuity of VE-cadherin-based junctions in the plaque surface endothelium compared to healthy vasculature. Furthermore, the vascular areas of disorganized VE-cadherin junctions were enriched with intravenously administered fluorescent nanoparticles, indicating extravasation through leaky junctions. Interestingly, advanced plaques displayed a more normalized junctional profile and lower levels of extravasated nanoparticles compared to early lesions.

Collectively, our previous findings suggest that the endothelial remodeling in atherosclerosis is not a one-directional process but involves both aggravation and normalization mechanisms. Driven by this hypothesis, we here aim to compare the morphological and ultrastructural characteristics in early and advanced atherosclerotic plaques, with a special focus on endothelial junction differences. Furthermore, we study the immune cell-endothelial cell interactions to provide functional insights into the *in vivo* mechanism of leukocyte recruitment to the atherosclerotic lesion site. Finally, we provide a clinical context, by performing ultrastructural analysis of the human carotid plaque surface.

2. Materials and methods

2.1. Experimental animals

For the SEM study, we investigated the early and advanced stage of atherosclerosis in eight C57BL6 *apoe*−/− mice (Charles River Laboratories, Beerse, Belgium). The included animals where either on a normal chow diet and high-fat diet (TD.88137, Envigo, Alconbury Huntington, UK). Two 18 week-old mice on chow diet and two 14-week old mice on 6-week high-fat diet were assigned into the early atherosclerosis group (Supplementary Table S1). The advanced atherosclerosis group consisted of two 30 weeks-old mice on chow diet and two 20 weeks-old mice on 12-week high-fat diet (Supplementary Table S2). For immune-gold labeling experiment, we used two additional *apoe*−/− mice with early and advanced plaques. To examine the normal aortic endothelium, we used one C57BL6 wild-type mouse (Charles River Laboratories). For confocal microscopy experiments, we used one C57BL6 wild-type mouse and *apoe*−/− mice on either 6-week (early atherosclerosis) or 12-week high-fat diet (advanced atherosclerosis) (four/group). The animals were sacrificed by either chemical anesthetic or carbon dioxide overdose, and perfused with PBS, containing 1 mM MgCl2 and CaCl2 (PBS++, room temperature). The aortas were excised and processed adequately to the readout method. All mouse experiments were performed in accordance with protocols approved by the Animal Experiment Committee of the Amsterdam University Medical Center in Amsterdam, Netherlands.

2.2. Human specimens

Two plaques from the Carotid Plaque Imaging Project (CPIP, Lund University) cohort, which consists of patients undergoing carotid endarterectomy (CEA) at the Vascular Department of Skåne University Hospital (Malmö, Sweden), were included. The study was approved by the local Regional Ethical Committee (reference number 472/2005) and written informed consent was given by the included patient. The study fully conforms to the principles of the Declaration of Helsinki. Indications to surgery were as described previously (Asciutto 2013, PMID: 23747086) with the degree of stenosis assessed with ultrasound based on flow velocities as previously validated (Hansen 1996, PMID: 8896476). Both patients were males and symptomatic, *i.e.* had >70% carotid artery stenosis associated with ipsilateral symptoms (amaurosis fugax, transient ischemia attack or stroke in the 6 months prior to surgery) as evaluated by a neurologist (whereas asymptomatic patients are defined as having >80% carotid artery stenosis, but have experienced no ipsilateral symptoms). The degree of stenosis was >95%. One patient had no history of diabetes or hypertension and no prior use of statins. The other patient had no history of diabetes, but a prior diagnosis of hypertension and had recently started treatment with statins (10 days prior). Further clinical characteristics of patients is summarized in Supplementary Table S3. The patients received heparin intraoperatively (~2500 IU). After clamping of the external, internal and common carotid, the artery was opened and flushed gently with saline to improve visibility. Immediately after surgical removal, the following regions were dissected from the plaque and placed in McDowell Trump's Fixative (4% PFA and 1% glutaraldehyde) (Electron Microscopy Sciences, Hatfield, PA, USA): 1) Carotis communis, 2) the carotid bulb region; the largest stenotic point outside the plaque rupture location, 3) the carotid bulb region; the largest stenotic point at the plaque rupture location, 4) Carotis interna, 5) Carotis externa, and 6) the 3 flow divider of the carotid bifurcation. Samples were further analyzed by the Department of Medical Biochemistry, Amsterdam University Medical Centers (Amsterdam, The Netherlands). They were processed for SEM analysis, using the same protocol as for mouse specimens, as described below.

2.3. En face analysis of mouse aorta and human plaques by SEM and morphological definitions

The collected vessels were treated with McDowell Trump's fixative (Electron Microscopy Sciences), which served also as a storage solution. The vessel samples were cut-open, pinned to cork rings and dehydrated using increasing ethanol concentrations *i.e.*, 50%, 70%, 80%, 90%, 96% (20 min incubation in each) and 100% (30 min). To reduce the sample surface tension, the samples were immersed in hexamethyldisilizane (Sigma-Aldrich) for 30 min and air-dried. Before imaging, tissues were mounted on aluminum SEM stubs using Leit-C conductive carbon cement (PLANO GmbH, Germany) and sputter-coated with a 4 nm-thick platinum-palladium layer using a Leica EM ACE600 sputter coater (Leica Microsystems, Illinois, USA). Images were acquired at 2 kV using a Zeiss Sigma 300 SEM (Zeiss, Germany) at different magnifications, ranging from 50-10,000× . In mouse specimens, early plaques were defined on SEM as small, bulging lesions with a diameter of up to 200 μm in 18 week-old *apoe*−/− mice on chow diet and in 14 week-old mice that received high-fat diet for 6 weeks before the sacrifice. Advanced plaques were ~1 mm in diameter in ~30 week-old mice on chow diet and in 20

week-old mice that received high-fat diet for 12 weeks before the sacrifice. Based on the height and surface morphology, we defined two areas within advanced plaques: 1) the advanced plaque body (central apical surface) and 2) shoulder region, the latter characterized by a high immune cell activity and/or the activated endothelium, i.e., the elongated cell shape, erected nuclei and bulging cell membranes. In addition to the surface analysis, the incidental tissue artefacts, as presented in Supplementary Fig. S1, allowed us to confirm e.g. the 'spongy' foam cell ultrastructure in the plaque interior. The endothelial junction phenotype was analyzed semiquantitative, by inspecting multiple plaque areas at 2,000 × magnification, and using frequency scoring system (-: absence, +: low, ++: medium and +++: high frequency). Measurements of para- and transcellular openings in endothelial layer were performed by placing a linear ROI across the longest dimension of an ultrastructure, using Fiji software. Paracellular openings were defined as discontinuities in endothelial cell-cell contact, in which smooth membrane edges of two neighboring cells were clearly separated. Transcellular openings were defined as gaps in the membrane of a single endothelial cell. The openings that displayed unclear features were not included in the analysis. In mice, endothelial necrotic areas were characterized by cell membrane thinning and numerous perforations, as presented in Supplementary Fig. S2. In human samples, thrombosis was defined as denuded area with one or several following components: fibrin, platelets and/or red blood cells. Morphologically different plaque areas were measured by manual ROI drawing in Fiji. The diameter of necrosis- (mouse) and thrombosis (human) associated openings was measured in the same way, as mentioned above. The average density of different types of openings was based on count in 3–5 representative images at 1000× magnification. In total, we have analyzed 819 mouse and 1889 human endothelial openings.

2.4. En face analysis of mouse aorta by immuno-SEM

The immunogold-labeling SEM (immuno-SEM) protocol involved 24 h incubation in 4% PFA in PHEM buffer. The fixed vessels were cut-open and pinned to the silicon-coated dish. They were washed two times with 0.15 M glycine in PBS, followed by 5 min incubation in 1% BSA in PBS. Subsequently, anti-CD11b rat anti-mouse antibody (clone:M1/70.15, Invitrogen) was added at 1:50 dilution. After overnight incubation, the samples were washed five times, each time by incubating for 3 min in 0.15 M glycine in PBS, and one time in 0.1% BSA in PBS. Subsequently, the samples were incubated with a bridging rabbit anti-rat antibody that binds protein A (Jackson ImmunoResearch, AffiniPure Rabbit Anti-Rat IgG + IgM (H + L), dilution: 1:200 in 1% BSA in PBS) for 30 min. This was followed by washing in 0.15 M glycine in PBS (five times for 3 min). Next, the vessels were incubated for 2 h with 10-nm protein A-gold nanoparticles, kindly provided by the Cell Microscopy Core, Department of Cell Biology, UMC Utrecht. Gold nanoparticles were diluted at 1:50 in 1% BSA in PBS. After three times wash in PBS, the samples were incubated for 5 min in 1% glutaraldehyde in PBS and washed another three times in PBS. Subsequently, the samples were rinsed in distilled water for 10 min and dehydrated by incubating in increasing concentrations of ethanol, as described above. Finally, the tissues were incubated for 30 min in hexamethyldisilizane and air-dried. The processed samples were mounted on an aluminum stub with a layer of conductive carbon cement (Plano GmbH). A 4 nm-thick carbon layer was evaporated on top of the samples using the Leica EM ACE600 sputter coater. SEM images were acquired using ZEISS Sigma 300 field emission scanning electron microscope at 5 kV using the back-scatter detector, HDBSD.

2.5. En face analysis of mouse aorta by confocal microscopy

For confocal microscopy, the arches were fixed in 4% paraformaldehyde (PFA) in PBS++ (with Mg2+ and Ca2+) for 12 min and, subsequently, stored in PBS ++ until staining. The mouse aortic arch was cut into two pieces, cut-open and immobilized on the silicon-coated Petri dish by means of 0.1 mm-thin pins. The tissue was permeabilized with 0.5% Triton X-100 in PBS for 10 min, washed and blocked with 2% bovine serum albumin (BSA) in PBS for 30 min. Subsequently, the vessels were incubated for 24 h at 4 °C with the following primary antibodies: polyclonal goat anti-mouse VE-cadherin antibody (Novus Biologicals; 1:100 dilution), either rat anti-mouse CD107b antibody (BD Pharmingen; clone M3/84; 1:100 6 dilution) or rat anti-mouse CD11b (ThermoFisher Scientific; clone M1/70, 1:100 dilution). After washing with 0.5% BSA in PBS, the secondary antibodies were added: Alexa Fluor 594-conjugated chicken anti-goat and Alexa Fluor 488-conjugated donkey anti-rat (both ThermoFisher Scientific; dilution 1:500), for 1 h at room temperature. The cell nuclei were stained with 2 μg/mL of 4',6-diamidino-2-phenylindole (DAPI) for 10 min. The stained vessels were mounted in a drop of Mowiol on microscope slides, with the endothelium facing up. A round glass coverslip was then placed on the top and lightly pressed to flatten the surface. Confocal microscopy was performed by using Leica TCS SP8 confocal laser scanning microscope (Leica Microsystems, Wetzlar, Germany), equipped with CS2 63x/1.40 oil objective, 470–670 nm Argon lasers and 405 nm UV Diode. The localization of atherosclerotic lesions was based on MAC-3/CD11b signal. In each vessel, multiple lesions were visualized. Image z-stacks were acquired through the endothelium, at x, y- and z-plane resolution of 0.2 and 0.5 μm, respectively, and the entire lesion volume at x,y- and z-plane resolution of 0.2 and 5 μm, respectively.

2.6. Statistical analysis

The frequency scores of mouse endothelial phenotypes were compared between different atherosclerotic areas (early plaque, advanced plaque body and advanced plaque shoulder) by using non-parametric Kruskal-Wallis test and Dunn's post-hoc analysis. The normality of quantitative variables, *i.e.*, the density and largest diameter of endothelial openings, and immune cell density, was tested with the Shapiro-Wilk test [20]. Since the hypothesis of normal distribution was rejected for many test groups, the multi-group comparison was performed with non-parametric Kruskal-Wallis test and Dunn's post-hoc test. The same analysis was used for both the mouse (inter-lesion analysis) and human data (intra-lesion analysis). The comparison between the para- and transcellular openings' size and density within the early or shoulder region was tested with non-parametric Mann-Whitney test. The comparison between the para-, transcellular and necrosis-associated openings within the advanced plaque body was performed with Kruskal-Wallis and Dunn's tests. All statistical analyses were performed in IBM SPPS Statistics 26. The differences were considered statistically relevant at $p < 0.05$.

3. Results

3.1. Endothelial cell-cell junctions in apoe$^{-/-}$ mice

The understanding of endothelial pathology first requires the evaluation of normal endothelium. Therefore, we perfused with phosphate buffered saline, excised and *ex vivo* fixed aorta of a wild-type C57BL/6 mouse, and examined with *en face* SEM. As presented in Fig. 1A and Supplementary Fig. S3A, on low-magnification SEM images, the endothelium appeared as a smooth and continuous tissue layer. Endothelial cell boundaries were barely visible, an indication of intact cell-cell junctions. The identified junctions displayed a diverse morphology (Fig. 1A and Supplementary Fig. S3B).

Representative images of arterial endothelial surface in *apoe*$^{-/-}$ mice, acquired in the aortic arch, are shown in Fig. 1B-E and Supplementary Fig. S4–S7. The early and advanced plaques were defined based on the mouse diet regimen and lesion size, which we summarize in Tables S1 and S2. Furthermore, within the advanced plaques, we differentiate two morphologically distinct areas: 1) the advanced plaque body (central apical surface) and 2) the shoulder region. The lesion-free endothelium

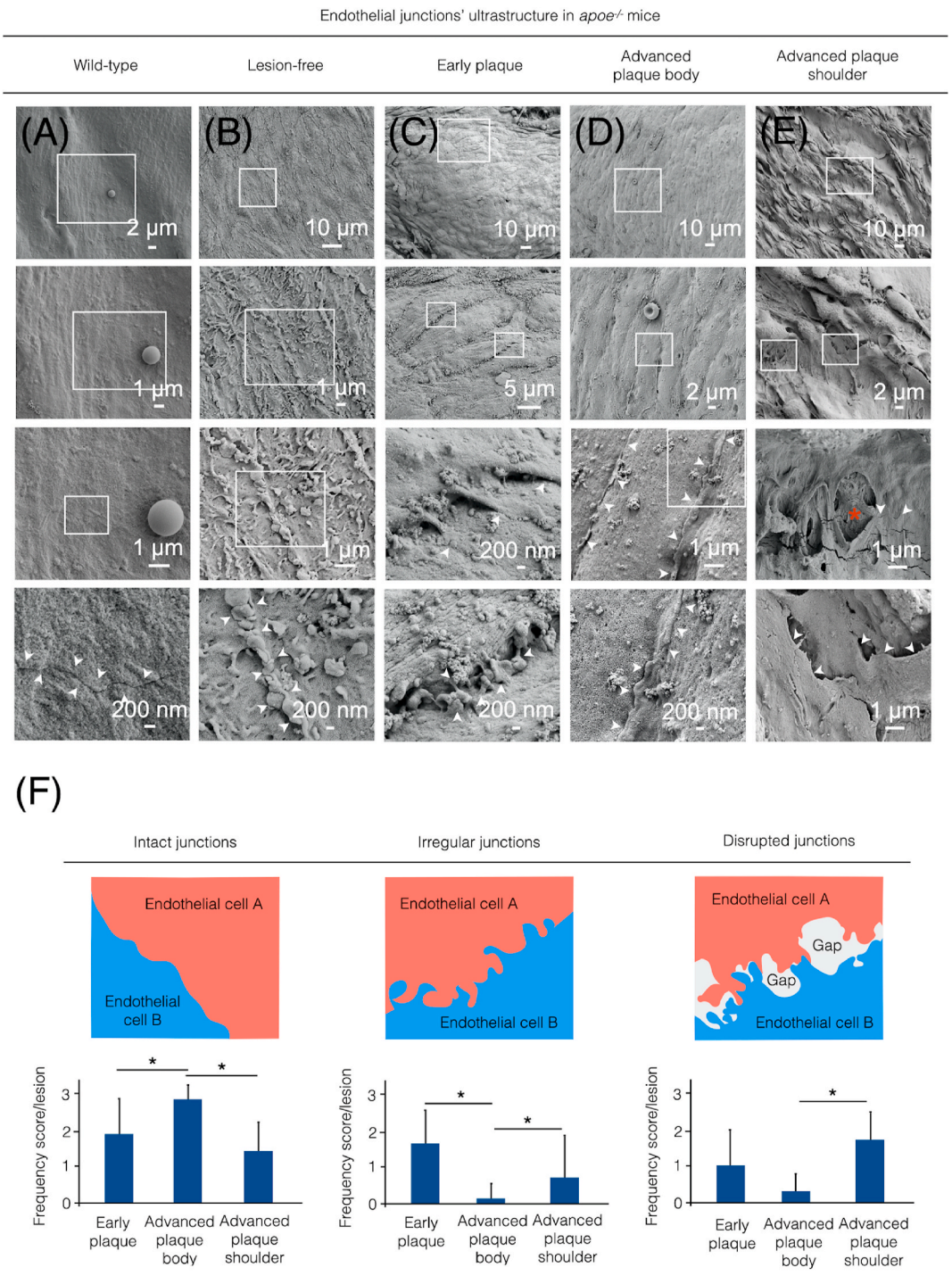

Fig. 1. Scanning electron microscopy of endothelial cell-cell junctions in wild-type and *apoe*$^{-/-}$ mice.
Representative scanning electron microscopy (SEM) images of the arterial endothelial surface in (A) wild-type and (B–E) *apoe*$^{-/-}$ C57BL6 mice on either (C) 18-week or (B,D,E) 30-week chow diet. In each panel, the same area is displayed at different magnifications. White arrowheads point at endothelial cell-cell contacts, while red asterisks define the gaps bigger than 500 nm, exposing subendothelial layer with different morphology compared to endothelial cell membrane. (F) In the upper panel, schematic representation of three main junctional morphologies we define in *apoe*$^{-/-}$ mouse endothelium: (1) intact junctions, which displayed well adherent endothelial cell membranes, (2) irregular junctions, characterized by chaotic cell-cell contacts rich in small membrane extensions, (3) disrupted junctions with paracellular gaps and exposed subendothelial ultrastructure. In the lower panel, the summary of frequency scores of intact (left), irregular (middle) and disrupted (right) endothelial junctions in different atherosclerotic areas, *i.e.*, early plaques, advanced plaques' body and shoulder regions. The frequency was scored between 0 (absent) and 3 (high frequency). Bars represent mean±standard deviation (SD). '*' indicates significant difference at $p < 0.05$, Kruskal-Wallis test with Dunn's *post hoc* test. (For interpretation of the references to color in this figure legend, the reader is referred to the Web version of this article.)

appeared as flat cell layer with thickened cell boundaries and densely protruded cell surface (Fig. 1B, Supplementary Figs. S4A and B). The atherosclerotic plaques displayed great diversity in the endothelial junctional ultrastructure (Fig. 1C-E). We observed three main junctional phenotypes: 1) intact, 2) irregular and 3) disrupted junctions (Fig. 1F). The intact junctions, displayed well adherent endothelial cell membranes as shown in Fig. 1D. The irregular junctions were characterized by chaotic small membrane extensions or thin membrane projections (microvilli-like) connecting neighboring endothelial cells (Fig. 1C). The disrupted junctions included paracellular gaps and exposed subendothelial ultrastructure (Fig. 1E). More examples of these endothelial cell-cell junction types can be found in Supplementary Fig. S8.

By employing the frequency scoring system, we compared the endothelial junctions of early lesions (n = 11), and the body and shoulder region of advanced plaques (n = 7), which is summarized in Fig. 1F and Supplementary Table S4. In early lesions, we identified highly heterogenous endothelial lining with a high contribution of both intact and irregular junctions, and, in seven lesions, we found the disrupted junctions. Both the irregular and disrupted phenotypes were rare on the advanced plaque body. Intact junctions were however significantly more prevalent compared to both early plaques ($p = 0.021$) and the shoulder region ($p = 0.002$). The highest frequency of disrupted junctions we report for the advanced plaque shoulder, which was significantly higher compared to low scores at the plaque body ($p = 0.003$).

To corroborate our SEM data, we studied the VE-cadherin organization by *en face* fluorescence microscopy. Both the wild-type (Supplementary Figs. S3C and D) and lesion-free *apoe*$^{-/-}$ endothelium (Supplementary Figs. S4C and D) displayed continuous, linear and non-linear VE-cadherin junctions. Early plaques, which were defined as highly MAC-3-positive lesions with a diameter of up to 200 μm, were rich in the remodeling endothelial junctions, characterized by numerous perpendicular VE-cadherin clusters (Supplementary Figs. S5E and H). The advanced lesions, identified by a thin (single-cell) layer of subendothelial macrophages and primarily acellular core, were covered by elongated endothelial cells with continuous and linear VE-cadherin junctions (Supplementary Fig. S6E-H). The shoulder region displayed abnormal VE-cadherin organization (Supplementary Fig. S7E-H). In the leukocyte-rich areas, we found very elongated endothelial cells and nuclei (Supplementary Fig. S7E-G). VE-cadherin junctions were thin or 'disappearing'. We also identified areas negative for CD11b staining, which displayed a disrupted VE-cadherin architecture (Supplementary Fig. S6F).

3.2. Endothelial openings in *apoe*$^{-/-}$ mice

The para- and transcellular endothelial openings have been previously identified in the inflamed vasculature and have been linked to both the systemic and local immune cell activity [20–22]. Our SEM data show a high incidence of abnormally large pores, *i.e.*, larger than 500 nm, on the surface of both early and advanced atherosclerotic plaques (Fig. 2). In general, the identification of endothelial openings/gaps was based on the morphological differences between the endothelial cell membrane and subendothelial layers, *i.e.*, smooth *versus* grainy (Fig. 2A, middle image, lower red asterisk), as well as the contrast generated by height differences, e.g., hollow openings in the upper image, Fig. 2B. The paracellular openings were defined as discontinuities in the endothelial cell-cell contact, in which smooth membrane edges of neighboring cells were clearly separated. The transcellular openings were defined as gaps in the membrane of a single endothelial cell. In necrotic endothelial areas, in which cell membranes were thin and heavily perforated (Supplementary Fig. S2), the identification of cell-cell junctions was frequently not possible. Therefore, we considered the necrosis-associated openings as a separate type of endothelial gaps.

On average, the paracellular openings were between 1 and 8 μm and they were relatively frequent in early plaques and the advanced plaque shoulder, *i.e.*, 680+/-1100 and 1200+/-1500 gaps/mm^2, respectively. In contrast, they were rare in advanced plaque body, *i.e.*, 80+/-65 gaps/mm^2 (Fig. 2D, left panel). Therefore, in advanced atherosclerosis, the shoulder region, 37+/-17% of the total plaque area (Fig. 2E), is a 'hot-spot' of endothelial permeability.

The transcellular openings were between 0.6 and 3 μm in diameter and localized primarily in the perinuclear cell region and near cell-cell junctions. (Fig. 2B and D middle panel). Their density was similar to that of paracellular pores but the diameter was significantly smaller in all three atherosclerotic areas (Fig. 2D). Notably, they were larger than physiological clathrin-coated pits or caveolae.

Necrosis-associated openings are the third type of endothelial openings, which we identify on the advanced plaque body (Fig. 2C and D right panel). Endothelial cell necrosis, manifested on SEM as the cell membrane perforation and nuclear detachment (Supplementary Fig. S2) [23], was found in five out of seven advanced lesions and accounted for approximately 5+/-9% of the advanced plaque body (Fig. 2E). The pores were circa 3 μm, present at the density of 1800±2500 openings/mm^2, which was significantly higher compared paracellular openings in the plaque body ($p = 0.013$), but they are confined to relatively small foci.

3.3. Immune cell-endothelial cell interactions in *apoe*$^{-/-}$ mice

Leukocyte adhesion and endothelial transmigration are critical steps in the process of leukocyte recruitment to the vessel wall in atherosclerosis [22,24–26]. We captured these processes by SEM (Fig. 3A-C and Supplementary Fig. S9). The majority of immune cells that we identified as transmigrating, were located within the opened endothelial cell-cell junctions (Fig. 3A, Supplementary Fig. S9C). However, we also found some evidence of the transcellular transmigration pathway. As shown in the Supplementary Fig. S9D, an immune cell is located in a large transcellular opening, which neighbors an intact cell-cell junction. We need to stress, that we observed a multitude of immune cell-endothelial interactions with complex/unclear morphology, which we could not stratify. To verify the myeloid lineage of the endothelium-associated immune cells, we performed immuno-gold labeling of CD11b (Fig. 3D and Supplementary Fig. S10). The average immune cell count in 11 early lesions was 140 ± 116/mm^2 and included both transmigrating and adhered cells. In the advanced plaque body, we found only 5 ± 6 immune cells/mm^2 (n = 7). The advanced plaque shoulder was the most populated by the immune cells with the average density of 478 ± 255 immune cells/mm^2 (n = 7), which is significantly higher compared to both early lesions and the advanced plaque body (Fig. 3C).

3.4. The surface ultrastructure of human advanced carotid plaques

SEM analysis of two human carotid plaques revealed their highly heterogeneous surface morphology (Fig. 4A). In both patients, endothelial areas displayed both the disrupted (Fig. 4B) and normalized junctional architecture (Supplementary Fig. S11), similar to that observed in mouse specimens. In disrupted areas, we find equally abundant para- and transcellular openings (Fig. 4B and C), with the average size of 2.5 and 1 μm, respectively (Fig. 4F). Furthermore, we identify large areas of highly disrupted endothelium with the average pore diameter of 6 and 10 μm in patient 1 and 2, respectively (Fig. 4D and F). In contrast to the murine model, the human plaque surface was rich in thrombosis, namely 80 and 62% in the examined samples. The fibrin, one of the key thrombotic components, displayed either tight or porous ultrastructure (Supplementary Fig. S12). In the latter case, the pores were ~1–2 μm in diameter and significantly denser compared to para- and transcellular endothelial openings in patient 2. Immune cells were localized both in endothelial and thrombotic areas (Supplementary Fig. S13).

In summary, SEM imaging of aortic endothelium in *apoe*$^{-/-}$ mice demonstrates its dramatic transformations during atherosclerosis

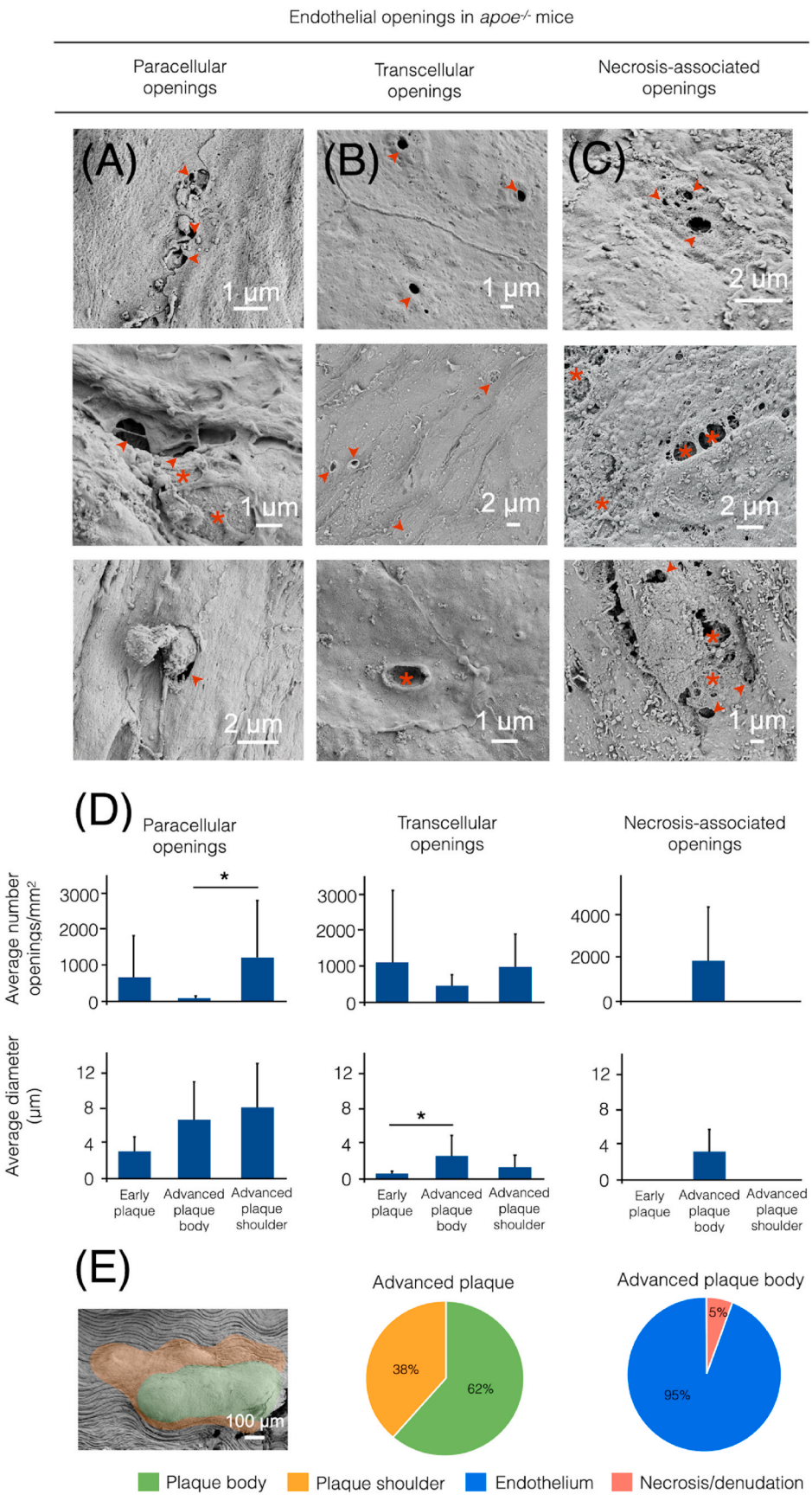

Fig. 2. Endothelial openings in *apoe*$^{-/-}$ mice. Representative scanning SEM images of (A) paracellular, (B) transcellular and (C) necrosis-associated endothelial openings in *apoe*$^{-/-}$ mice. White arrowheads point at smaller pores, while red asterisks define large openings with exposed sub-endothelial layers. The images were acquired in mice on 18- (upper B) and 30-week chow diet (upper, middle C, middle and lower B), and 6- (lower A) and 12-week high-fat diet (lower C, upper and middle A). (D) The average density and diameter of paracellular (left panel), transcellular (middle panel) and necrosis-associated (right panel) endothelial openings in different atherosclerotic areas. Bars represent mean±standard deviation (SD). '*' indicates significant difference at $p < 0.05$, Kruskal-Wallis test with Dunn's *post hoc* test. (E) Representative image of advanced plaque with the colored body and shoulder region in green and orange, respectively. Pie charts represent the average fraction of plaque body and shoulder in advanced mouse lesions, and the fraction of endothelial cell necrosis. (For interpretation of the references to color in this figure legend, the reader is referred to the Web version of this article.)

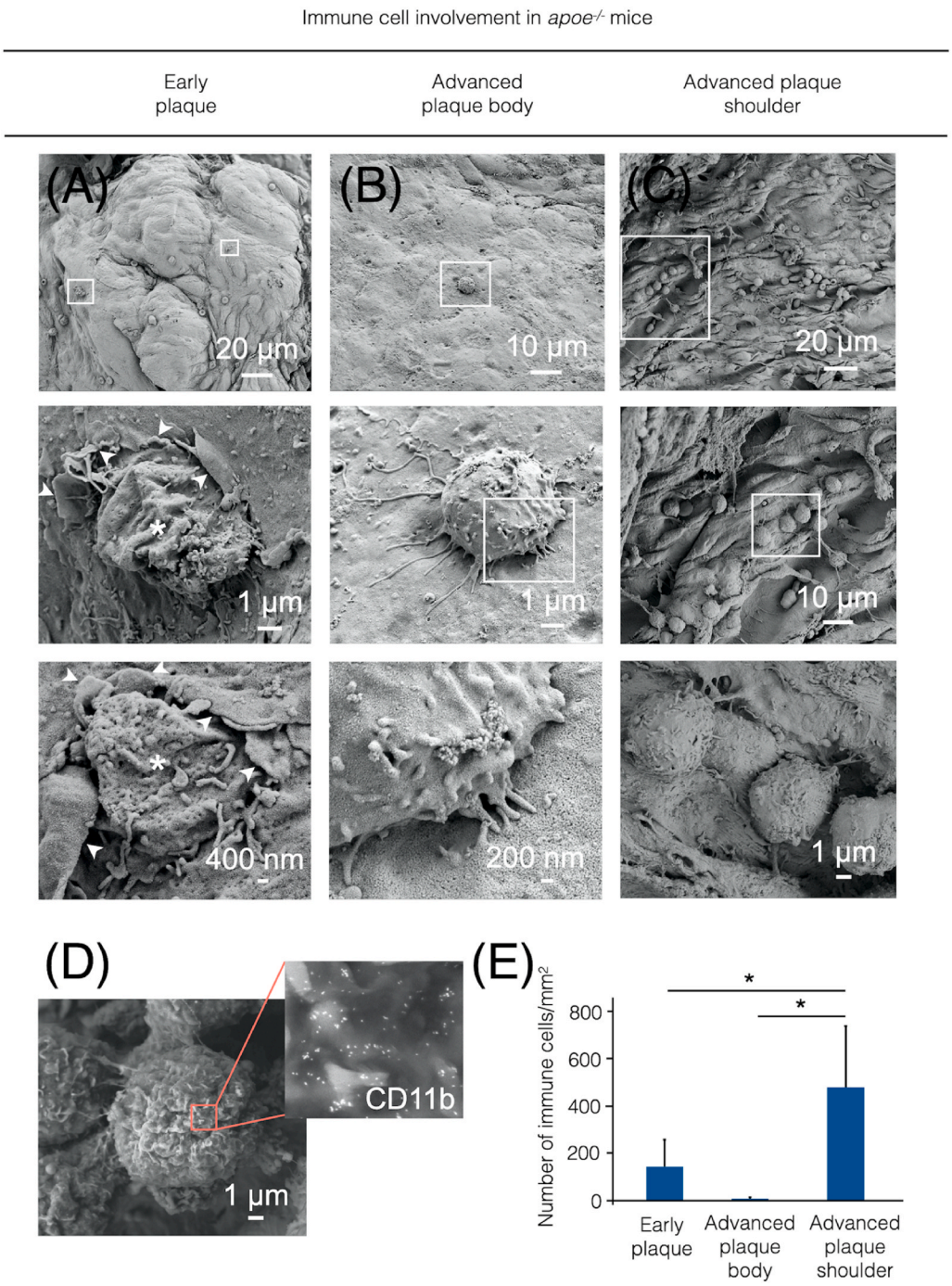

Fig. 3. Immune cells on the plaque surface of *apoe*$^{-/-}$ mice.
(A) Images of an early plaque (18-week chow diet) with two transmigrating immune cells (white ROIs), which are shown at high magnification in the lower and middle panel. White arrowheads indicate the lifted endothelial cell edges and asterisks mark the immune cells. In (B) and (C) (both 30-week chow diet), different magnifications of the advanced plaque body and shoulder region are respectively shown, both with adhered immune cell(s). (D) SEM image of CD11b-positive leukocyte labeled with 10 nm gold nanoparticles. (E) The immune cell density on the surface of different atherosclerotic areas. Bars represent mean±standard deviation (SD). '*' indicates significant difference at $p < 0.05$, Kruskal-Wallis test with Dunn's *post hoc* test. (For interpretation of the references to color in this figure legend, the reader is referred to the Web version of this article.)

development. Early atherosclerotic plaques display junctional abnormalities and/or large transcellular pores. Intriguingly, when atherosclerotic plaques progress, the endothelium seems to regenerate, as shown by intact cell-cell junction ultrastructure. This junctional normalization goes hand in hand with low immune cell adhesion. In advanced lesions, the plaque shoulder displays a highly activated endothelial phenotype and leukocyte recruitment. Our results reveal a highly heterogeneous and dynamic endothelial landscape in the development of atherosclerosis (Fig. 5), which opens a window of opportunity to normalize the endothelium and counteract atherosclerosis. Furthermore, our findings in human carotid plaque specimens confirm the coexistence of both endothelial patterns in clinically evident and advanced atherosclerosis.

4. Discussion

The current study gives unique insights into directions of arterial endothelial remodeling during atherogenesis. The revealed normalization of endothelial lining and few signs of leukocyte adhesion in the body of the plaque might be a consequence of intimal remodeling, the body's effort to stabilize the atherosclerotic plaque and blood flow patterns. The initially proteoglycan-rich extracellular matrix (ECM) is transformed into the collagen-rich ECM by proliferating synthetic vascular smooth muscle cells (VSMCs) [27]. The collagen microenvironment seems to be more comparable to physiological conditions where endothelial cells overlay elastin and VSMC layers. We also consider the impact of subendothelial oxLDL, which in an *in vitro* model, has shown to downregulate VE-cadherin in endothelial cell-cell

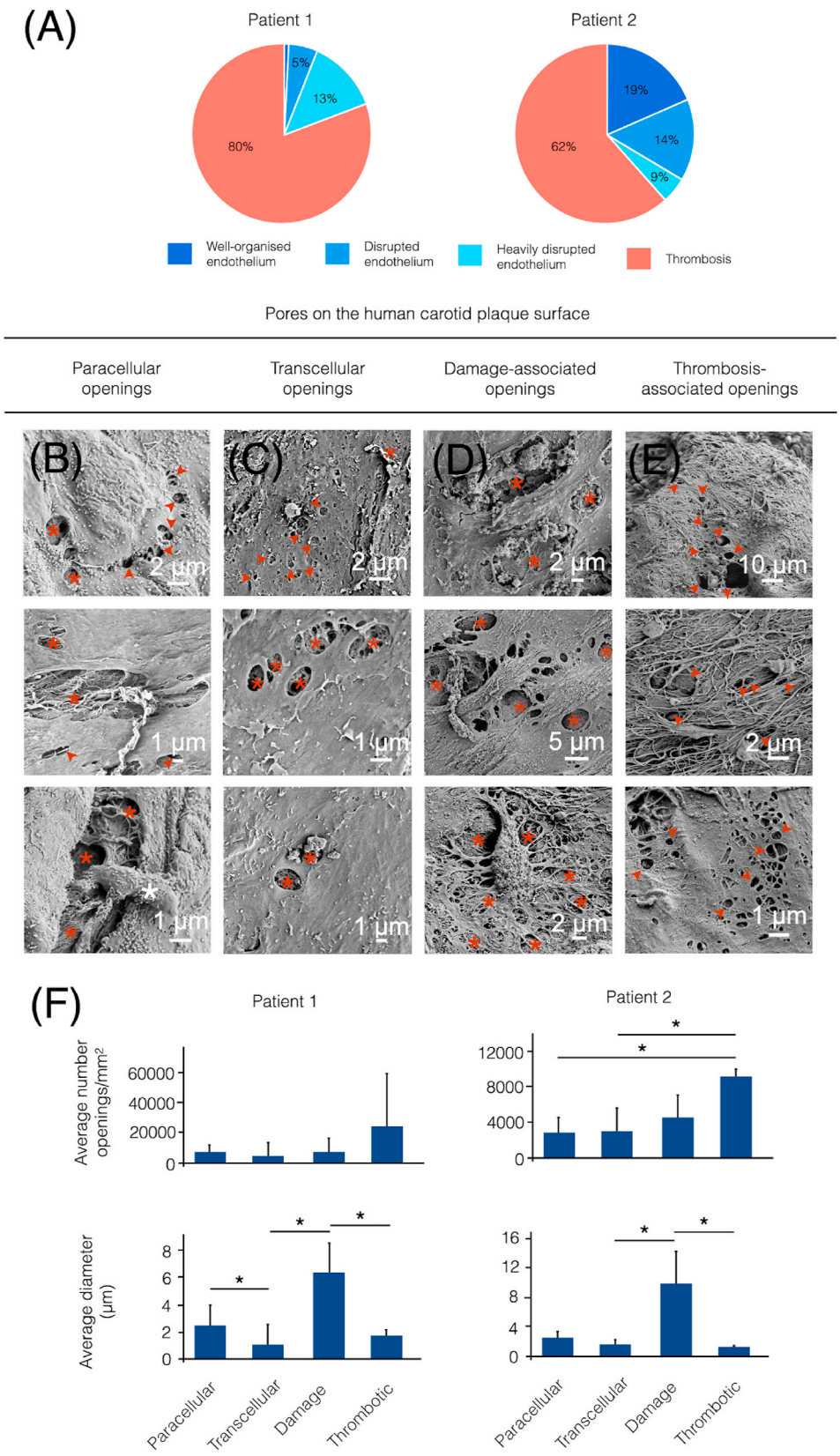

Fig. 4. SEM analysis of human carotid plaques. (A) Pie charts displaying the percentage of well-organized, disputed and heavily-disrupted endothelium, and thrombosis in two human carotid plaques. (B and C) Example SEM images of endothelial openings on the human plaque surface: (B) paracellular, (C) transcellular, and (D) openings in highly disrupted/damaged endothelial areas, where endothelial cell-cell junctions cannot be easily identified, and (E) thrombosis-associated pores. (F) The average density (upper panel) and diameter (lower panel) of paracellular, transcellular, and damage-associated (in highly disrupted endothelial areas) endothelial openings and thrombosis-associated pores in two patients. Bars represent mean±standard deviation (SD) (n = 5 representative images at 1000×). '*' indicates significant difference at $p < 0.05$, Kruskal-Wallis test with Dunn's *post hoc* test.

junctions [28], and which is more prevalent in early lesions compared to advanced counterparts [29]. The plaque's body is also the most luminal bulging part of the lesion, experiencing relatively higher shear stress compared to the lower shoulder region, which possibly contributes to the endothelial normalization [30]. This phenomenon occurs in conjunction with a significantly lower leukocyte adhesion, being in line with the findings of Robbins et al. [31], who previously demonstrated that advanced plaques feature less leukocyte recruitment, but more

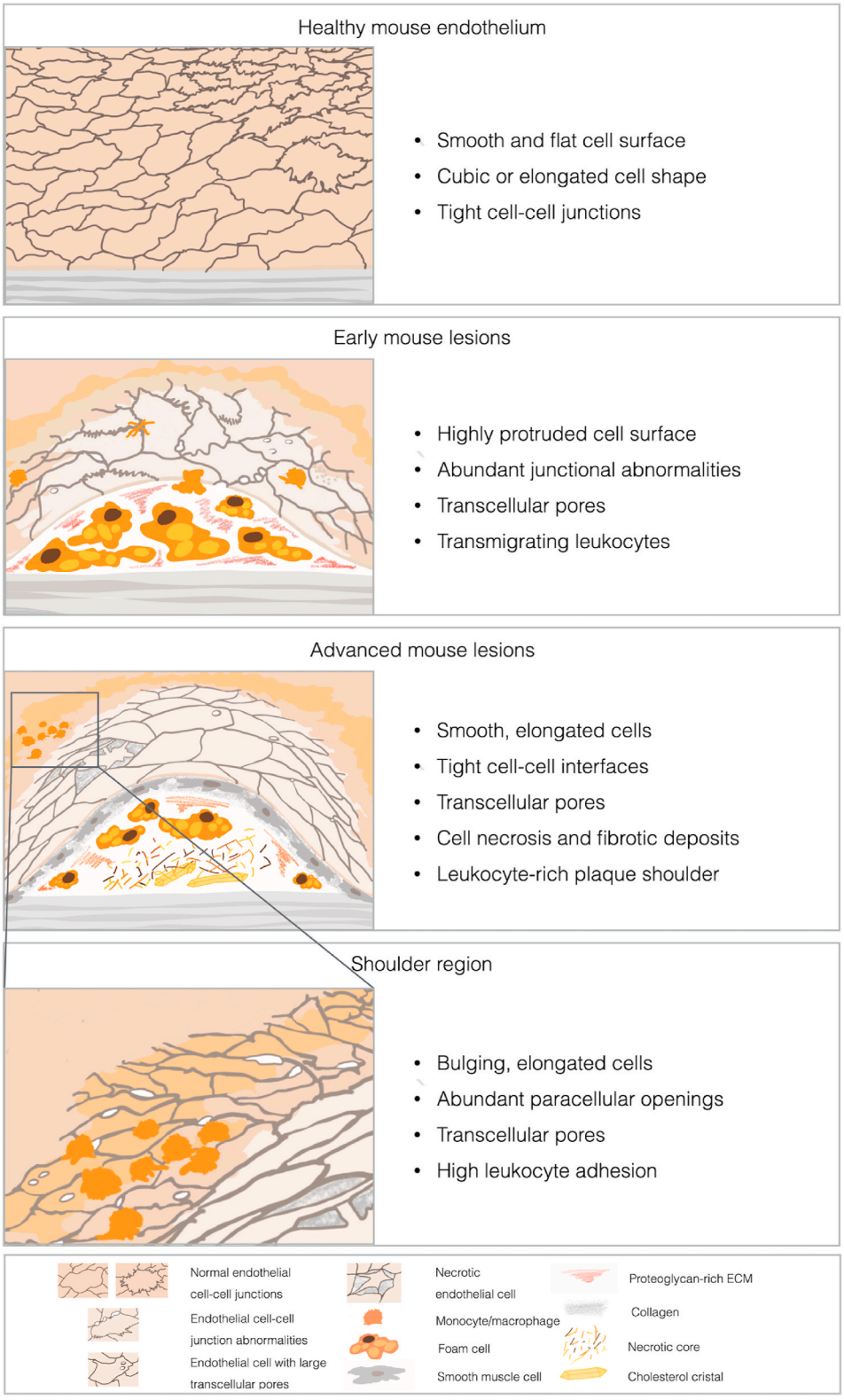

Fig. 5. Schematic summary of SEM finding in apoe$^{-/-}$ mice.
The formation of early atherosclerotic lesions leads to the endothelial barrier remodeling and disruption (second panel), while the plaque maturation processes are associated with both the endothelial normalization on the plaque body (third panel) and aggravation at the shoulder region (fourth panel). The normal mouse arterial endothelium is depicted in the first panel. All drawn structures are explained in the legend below.

intraplaque macrophage proliferation. Importantly, the preserved endothelial areas on human plaques share generally the same characteristics as murine specimens. This suggests that our pre-clinical findings might have translation to the human plaque progression/expansion mechanism.

Although the endothelium covering the plaque's body appears normalized in advanced disease, the shoulder region displays highly disrupted and/or activated endothelial morphology, and abnormal VE-cadherin organization (Supplementary Fig. S7E-H). It emerges as a critical area of inflammatory cell adhesion with abundance of para- and transcellular endothelial openings. Previously, studies on human atheromas identified the plaque shoulder as a frequent site of plaque rupture [32]. This has been attributed to a relatively thin fibrous cap and high inflammatory activity in this region. In *apoe*$^{-/-}$ mice, spontaneous

thrombotic events are rare, therefore, we cannot make similar extrapolations. Nevertheless, our findings support the established thesis on the plaque shoulder as a critical site of immune cell activity in advanced atherosclerosis.

Another relevant feature in advanced mouse atherosclerosis is endothelial necrosis, representing few percent of the total plaque surface and leading to the endothelial pore formation (Fig. 2C-E). In human atherosclerosis, we find highly disrupted endothelial areas, which however do not carry necrotic characteristics. Importantly, human plaques display extensive surface thrombosis, which porous ultrastructure might mimic the endothelial hyperpermeability and interfere with the permeability data interpretation (Fig. 5A and Supplementary Fig. S12). Considering our initial SEM findings as well as the previous histopathological and imaging studies [33,34], the plaque surface thrombosis seems to be very common in humans. However, its extent and maturity might vary greatly between different lesions and subjects. SEM is an excellent imaging tool to further improve our knowledge on the size, type and spatial distribution of surface thrombosis in different patient groups since it enables studying large surface areas at a superb spatial resolution of up to ~2 nm. By using SEM, we also find incidental endothelial denudations in both types of specimens (Supplementary Fig. S14). The relevance of denudation or superficial erosion as a thrombotic trigger has recently been highlighted by Libby and colleagues [7]. We anticipate that the SEM approach might underestimate endothelial denudation since any type of surface deposition, e.g., a thin layer of platelets, fibrin or red blood cells would cover the denuded areas. Nevertheless, our current findings suggest that the fully exposed, purely extracellular matrix-rich denudation is rare.

The aforementioned findings shed new light on our recent study in *apoe*$^{-/-}$ mice, which revealed significantly lower extravasation of nanoparticles to advanced lesions compared to early counterparts [19]. By performing SEM analysis, we were able to unveil the ultrastructural consequences of VE-cadherin remodeling *i.e.*, a dramatic ultrastructural reorganization and normalized phenotype of endothelial cell-cell junctions in early and advanced plaque body, respectively (Fig. 1). Furthermore, we showed alternative or complementary pathways for nanoparticle accumulation in the plaque, *i.e.*, via transcellular and necrosis-associated openings, which we were not able to identify with *en face* fluorescence microscopy.

The past few years brought new scientific evidence on the phenotypic and epigenetic specialization of endothelial cells in different organs [35]. Furthermore, recent single-cell RNA sequencing (scRNA-seq) studies have shown heterogeneity of endothelial cell population within pathologies, such as in the inflamed chondroid tissue [36] and tumors [37–39]. In cardiovascular research, scRNA-seq analyses evolve predominantly, but not exclusively, around immune cells [40,41]. In our study, we observe highly versatile atherosclerotic endothelium. Undisputedly, the entire lining is affected by the disease. However, the cell morphology and cell-cell connectivity varied between a relatively normal to a highly disturbed. This heterogeneity was observed both on the level of a single plaque and entire vessel. It seems therefore highly relevant to identify metabolic and epigenetic factors that predispose endothelial cells to either plaque stabilization or vulnerability.

Our results underline the spatial and temporal diversity of atherosclerotic endothelial landscape. The general term 'dysfunctional endothelium' or 'atherosclerotic endothelium' therefore requires reevaluation to underline the versatility of atherosclerosis-associated endothelial transformations. The revealed endothelial heterogeneity might be a relevant factor in the plaque stability and should be considered during the disease evaluation. Furthermore, it is of great importance to further characterize and, ultimately, therapeutically establish a normalized endothelial phenotype in atherosclerosis.

Financial support

We acknowledge the support from the Netherlands CardioVascular Research Initiative: the Dutch Heart Foundation, Dutch Federation of University Medical Centres, the Netherlands Organization for Health Research, and Development and the Royal Netherlands Academy of Sciences for the GENIUS-II project 'Generating the best evidence-based pharmaceutical targets for atherosclerosis' (CVON2017-20 to E.L.); the Deutsche Forschungsgemeinschaft (CRC 1123 to E.L., project A5); the Netherlands Organization for Scientific Research (NWO) for Vici grant to E.L. (016.130.676), Vici grant to W.J.M.M (016.176.622), Vidi grant to W.J.M.M (016.136.324) and S.H (016.156.327), STW grant (15851); the European Research Council (ERC consolidator grant to E.L), Swedish Research Council, Skåne University Hospital, Lund University Diabetes Centre-IRC to I.G., and Swedish Heart and Lung Foundation to I.G. and A.S. This work was financially supported by National Institutes of Health grants R01 HL118440 (W.J.M.M.), R01 HL125703 (W.J.M.M.), R01 CA155432 (W.J.M.M.). The authors also thank Sensi Pharma BV for their funding.

CRediT authorship contribution statement

Ewelina Kluza: Conceptualization, Methodology, Investigation, Writing – original draft, Visualization. **Thijs J. Beldman:** Investigation, Methodology, Writing – review & editing. **Annelie Shami:** Investigation, Writing – review & editing. **Edwin R. Scholl:** Investigation, Methodology. **Tsveta S. Malinova:** Conceptualization, Writing – review & editing. **Anita E. Grootemaat:** Investigation. **Nicole N. van der Wel:** Supervision, Resources, Writing – review & editing. **Isabel Gonçalves:** Conceptualization, Supervision, Investigation, Writing – review & editing, Funding acquisition, Resources. **Stephan Huveneers:** Conceptualization, Supervision, Writing – review & editing, Funding acquisition, Resources. **Willem J.M. Mulder:** Supervision, Writing – review & editing, Funding acquisition, Resources. **Esther Lutgens:** Conceptualization, Supervision, Writing – review & editing, Funding acquisition, Resources.

Declaration of competing interest

The authors declare that they have no known competing financial interests or personal relationships that could have appeared to influence the work reported in this paper.

Acknowledgments

We thank Linda Beckers and Cindy P.A.A. van Roomen for help with the tissue processing.

Appendix A. Supplementary data

Supplementary data to this article can be found online at https://doi.org/10.1016/j.atherosclerosis.2021.11.017.

References

[1] M.A. Gimbrone Jr., G. García-Cardeña, Endothelial cell dysfunction and the pathobiology of atherosclerosis, Circ. Res. 118 (2016) 620–636, https://doi.org/10.1161/CIRCRESAHA.115.306301.
[2] A. Lerman, A.M. Zeiher, Endothelial function: cardiac events, Circulation 111 (2005) 363–368, https://doi.org/10.1161/01.CIR.0000153339.27064.14.
[3] C. Calcagno, Z.A. Fayad, Imaging the permeable endothelium: predicting plaque rupture in atherosclerotic rabbits, Circ. Cardiovasc. Imaging 9 (2016), https://doi.org/10.1161/CIRCIMAGING.116.005955.

[4] T.J. Anderson, Assessment and treatment of endothelial dysfunction in humans, J. Am. Coll. Cardiol. 34 (1999) 631–638, https://doi.org/10.1016/S0735-1097(99)00259-4.

[5] A. Farb, A.P. Burke, A.L. Tang, Y. Liang, P. Mannan, J. Smialek, R. Virmani, Coronary plaque erosion without rupture into a lipid core, Circulation 93 (1996) 1354–1363, https://doi.org/10.1161/01.CIR.93.7.1354.

[6] E. Arbustini, B. Dal Bello, P. Morbini, A.P. Burke, M. Bocciarelli, G. Specchia, R. Virmani, Plaque erosion is a major substrate for coronary thrombosis in acute myocardial infarction, Heart 82 (1999) 269, https://doi.org/10.1136/hrt.82.3.269. LP – 272.

[7] P. Libby, G. Pasterkamp, F. Crea, I.-K. Jang, Reassessing the mechanisms of acute coronary syndromes, Circ. Res. 124 (2019) 150–160, https://doi.org/10.1161/CIRCRESAHA.118.311098.

[8] P.C. Freiman, G.G. Mitchell, D.D. Heistad, M.L. Armstrong, D.G. Harrison, Atherosclerosis impairs endothelium-dependent vascular relaxation to acetylcholine and thrombin in primates, Circ. Res. 58 (1986) 783–789, https://doi.org/10.1161/01.RES.58.6.783.

[9] M.J. Davies, N. Woolf, P.M. Rowles, J. Pepper, Morphology of the endothelium over atherosclerotic plaques in human coronary arteries, Br. Heart J. 60 (1988) 459–464, https://doi.org/10.1136/hrt.60.6.459.

[10] Y. Kim, M.E. Lobatto, T. Kawahara, B.L. Chung, A.J. Mieszawska, B.L. Sanchez-Gaytan, F. Fay, M.L. Senders, C. Calcagno, J. Becraft, M.T. Saung, R.E. Gordon, E.S. G. Stroes, M. Ma, O.C. Farokhzad, Z.A. Fayad, W.J.M. Mulder, R. Langer, Probing nanoparticle translocation across the permeable endothelium in experimental atherosclerosis, Proc. Natl. Acad. Sci. Unit. States Am. 111 (2014) 1078–1083, https://doi.org/10.1073/PNAS.1322725111.

[11] A. Phinikaridou, M.E. Andia, G. Passacquale, A. Ferro, R.M. Botnar, Noninvasive MRI monitoring of the effect of interventions on endothelial permeability in murine atherosclerosis using an albumin-binding contrast agent, J. Am. Heart Assoc. 2 (2013), e000402, https://doi.org/10.1161/JAHA.113.000402.

[12] D.G. Sedding, E.C. Boyle, J.A.F. Demandt, J.C. Sluimer, J. Dutzmann, A. Haverich, J. Bauersachs, Vasa vasorum angiogenesis: key player in the initiation and progression of atherosclerosis and potential target for the treatment of cardiovascular disease, Front. Immunol. 9 (2018) 706. https://www.frontiersin.org/article/10.3389/fimmu.2018.00706.

[13] W.A. Muller, Leukocyte–endothelial-cell interactions in leukocyte transmigration and the inflammatory response, Trends Immunol. 24 (2003) 326–333, https://doi.org/10.1016/S1471-4906(03)00117-0.

[14] J.D. van Buul, P.L. Hordijk, Signaling in leukocyte transendothelial migration, Arterioscler. Thromb. Vasc. Biol. 24 (2004) 824–833, https://doi.org/10.1161/01.ATV.0000122854.76267.5c.

[15] T.J.C. Harris, U. Tepass, Adherens junctions: from molecules to morphogenesis, Nat. Rev. Mol. Cell Biol. 11 (2010) 502–514, https://doi.org/10.1038/nrm2927.

[16] E. Dejana, F. Orsenigo, M.G. Lampugnani, E. Dejana, W. Risau, The role of adherens junctions and VE-cadherin in the control of vascular permeability, J. Cell Sci. 121 (2008) 2115–2122, https://doi.org/10.1242/jcs.017897.

[17] T.S. Malinova, S. Huveneers, Sensing of cytoskeletal forces by asymmetric adherens junctions, Trends Cell Biol. 28 (2018) 328–341, https://doi.org/10.1016/j.tcb.2017.11.002.

[18] S. Huveneers, J. Oldenburg, E. Spanjaard, G. van der Krogt, I. Grigoriev, A. Akhmanova, H. Rehmann, J. de Rooij, Vinculin associates with endothelial VE-cadherin junctions to control force-dependent remodeling, J. Cell Biol. 196 (2012) 641–652, https://doi.org/10.1083/jcb.201108120.

[19] T.J. Beldman, T.S. Malinova, E. Desclos, A.E. Grootemaat, A.L.S. Misiak, S. van der Velden, C.P.A.A. van Roomen, L. Beckers, H.A. van Veen, P.M. Krawczyk, R. A. Hoebe, J.C. Sluimer, A.E. Neele, M.P.J. de Winther, N.N. van der Wel, E. Lutgens, W.J.M. Mulder, S. Huveneers, E. Kluza, Nanoparticle-aided characterization of arterial endothelial architecture during atherosclerosis progression and metabolic therapy, ACS Nano 13 (2019) 13759–13774, https://doi.org/10.1021/acsnano.8b08875.

[20] G. Majno, G.E. Palade, Studies on inflammation. 1. The effect of histamine and serotonin on vascular permeability: an electron microscopic study, J. Biophys. Biochem. Cytol. 11 (1961) 571–605, https://doi.org/10.1083/jcb.11.3.571.

[21] D.M. McDonald, G. Thurston, P. Baluk, Endothelial gaps as sites for plasma leakage in inflammation, microcirculation. https://doi.org/10.1111/j.1549-8719.1999.tb00084.x, 1999, 6, 7-22.

[22] A.C.I. van Steen, W.J. van der Meer, I.E. Hoefer, J.D. van Buul, Actin remodelling of the endothelium during transendothelial migration of leukocytes, Atherosclerosis 315 (2020) 102–110, https://doi.org/10.1016/j.atherosclerosis.2020.06.004.

[23] S.G. Levy, C.M. Kirkness, J. Moss, L. Ficker, A.C.E. McCartney, On the pathology of the iridocorneal-endothelial syndrome: the ultrastructural appearances of 'subtotal-ICE, Eye 9 (1995) 318–323, https://doi.org/10.1038/eye.1995.62.

[24] D. Schulte, V. Küppers, N. Dartsch, A. Broermann, H. Li, A. Zarbock, O. Kamenyeva, F. Kiefer, A. Khandoga, S. Massberg, D. Vestweber, Stabilizing the VE-cadherin-catenin complex blocks leukocyte extravasation and vascular permeability, EMBO J. 30 (2011) 4157–4170, https://doi.org/10.1038/emboj.2011.304.

[25] A. Woodfin, M.-B. Voisin, M. Beyrau, B. Colom, D. Caille, F.-M. Diapouli, G. B. Nash, T. Chavakis, S.M. Albelda, G.E. Rainger, P. Meda, B.A. Imhof, S. Nourshargh, The junctional adhesion molecule JAM-C regulates polarized transendothelial migration of neutrophils in vivo, Nat. Immunol. 12 (2011) 761–769, https://doi.org/10.1038/ni.2062.

[26] N. Heemskerk, L. Schimmel, C. Oort, J. van Rijssel, T. Yin, B. Ma, J. van Unen, B. Pitter, S. Huveneers, J. Goedhart, Y. Wu, E. Montanez, A. Woodfin, J.D. van Buul, F-actin-rich contractile endothelial pores prevent vascular leakage during leukocyte diapedesis through local RhoA signalling, Nat. Commun. 7 (2016) 10493, https://doi.org/10.1038/ncomms10493.

[27] A. Shami, I. Gonçalves, A. Hultgårdh-Nilsson, Collagen and related extracellular matrix proteins in atherosclerotic plaque development, Curr. Opin. Lipidol. 25 (2014) 394–399. https://journals.lww.com/co-lipidology/Fulltext/2014/10000/Collagen_and_related_extracellular_matrix_proteins.11.aspx.

[28] K. Hashimoto, N. Kataoka, E. Nakamura, K. Tsujioka, F. Kajiya, Oxidized LDL specifically promotes the initiation of monocyte invasion during transendothelial migration with upregulated PECAM-1 and downregulated VE-cadherin on endothelial junctions, Atherosclerosis 194 (2007), https://doi.org/10.1016/j.atherosclerosis.2006.11.029 e9–e17.

[29] N. Simionescu, A. Sima, A. Dobrian, D. Tirziu, M. Simionescu, in: A. Roessner, E. Vollmer (Eds.), Pathobiochemical Changes of the Arterial Wall at the Inception of Atherosclerosis BT - Recent Progress in Atherosclerosis Research, Springer Berlin Heidelberg, Berlin, Heidelberg, 1993, pp. 1–45, https://doi.org/10.1007/978-3-642-76849-1_1.

[30] K.S. Cunningham, A.I. Gotlieb, The role of shear stress in the pathogenesis of atherosclerosis, Lab. Invest. 85 (2005) 9–23, https://doi.org/10.1038/labinvest.3700215.

[31] C.S. Robbins, I. Hilgendorf, G.F. Weber, I. Theurl, Y. Iwamoto, J.L. Figueiredo, R. Gorbatov, G.K. Sukhova, L.M.S. Gerhardt, D. Smyth, C.C.J. Zavitz, E. A. Shikatani, M. Parsons, N. van Rooijen, H.Y. Lin, M. Husain, P. Libby, M. Nahrendorf, R. Weissleder, F.K. Swirski, Local proliferation dominates lesional macrophage accumulation in atherosclerosis, Nat. Med. 19 (2013) 1166–1172, https://doi.org/10.1038/nm.3258.

[32] F. Erling, P.K. Shah, F. Valentin, Coronary plaque disruption, Circulation 92 (1995) 657–671, https://doi.org/10.1161/01.CIR.92.3.657.

[33] A.P. Burke, F.D. Kolodgie, A. Farb, D.K. Weber, G.T. Malcom, J. Smialek, R. Virmani, Healed plaque ruptures and sudden coronary death, Circulation 103 (2001) 934–940, https://doi.org/10.1161/01.CIR.103.7.934.

[34] T. Saam, J. Cai, L. Ma, Y.-Q. Cai, M.S. Ferguson, N.L. Polissar, T.S. Hatsukami, C. Yuan, Comparison of symptomatic and asymptomatic atherosclerotic carotid plaque features with in vivo MR imaging, Radiology 240 (2006) 464–472, https://doi.org/10.1148/radiol.2402050390.

[35] J. Kalucka, L.P.M.H. de Rooij, J. Goveia, K. Rohlenova, S.J. Dumas, E. Meta, N. V Conchinha, F. Taverna, L.A. Teuwen, K. Veys, M. García-Caballero, S. Khan, V. Geldhof, L. Sokol, R. Chen, L. Treps, M. Borri, P. de Zeeuw, C. Dubois, T. K. Karakach, K.D. Falkenberg, M. Parys, X. Yin, S. Vinckier, Y. Du, R.A. Fenton, L. Schoonjans, M. Dewerchin, G. Eelen, B. Thienpont, L. Lin, L. Bolund, X. Li, Y. Luo, P. Carmeliet, Single-cell transcriptome atlas of murine endothelial cells, Cell 180 (2020) 764–779, https://doi.org/10.1016/j.cell.2020.01.015, e20.

[36] K. Rohlenova, J. Goveia, M. García-Caballero, A. Subramanian, J. Kalucka, L. Treps, K.D. Falkenberg, L.P.M.H. de Rooij, Y. Zheng, L. Lin, L. Sokol, L. A. Teuwen, V. Geldhof, F. Taverna, A. Pircher, L.-C. Conradi, S. Khan, S. Stegen, D. Panovska, F. De Smet, F.J.T. Staal, R.J. Mclaughlin, S. Vinckier, T. Van Bergen, N. Ectors, P. De Haes, J. Wang, L. Bolund, L. Schoonjans, T.K. Karakach, H. Yang, G. Carmeliet, Y. Liu, B. Thienpont, M. Dewerchin, G. Eelen, X. Li, Y. Luo, P. Carmeliet, Single-cell RNA sequencing maps endothelial metabolic plasticity in pathological angiogenesis, Cell Metabol. 31 (2020) 862–877, https://doi.org/10.1016/j.cmet.2020.03.009, e14.

[37] Q. Zhao, A. Eichten, A. Parveen, C. Adler, Y. Huang, W. Wang, Y. Ding, A. Adler, T. Nevins, M. Ni, Y. Wei, G. Thurston, Single-cell transcriptome analyses reveal endothelial cell heterogeneity in tumors and changes following antiangiogenic treatment, Cancer Res. 78 (2018) 2370, https://doi.org/10.1158/0008-5472.CAN-17-2728. LP – 2382.

[38] Z. Sun, C.Y. Wang, D.A. Lawson, S. Kwek, H.G. Velozo, M. Owyong, M.D. Lai, L. Fong, M. Wilson, H. Su, Z. Werb, D.L. Cooke, Single-cell RNA sequencing reveals gene expression signatures of breast cancer-associated endothelial cells, Oncotarget 9 (2017) 10945–10961, https://doi.org/10.18632/oncotarget.23760.

[39] J. Goveia, K. Rohlenova, F. Taverna, L. Treps, L.C. Conradi, A. Pircher, V. Geldhof, L.P.M.H. de Rooij, J. Kalucka, L. Sokol, M. García-Caballero, Y. Zheng, J. Qian, L. A. Teuwen, S. Khan, B. Boeckx, E. Wauters, H. Decaluwé, P. De Leyn, J. Vansteenkiste, B. Weynand, X. Sagaert, E. Verbeken, A. Wolthuis, B. Topal, W. Everaerts, H. Bohnenberger, A. Emmert, D. Panovska, F. De Smet, F.J.T. Staal, R.J. Mclaughlin, F. Impens, V. Lagani, S. Vinckier, M. Mazzone, L. Schoonjans, M. Dewerchin, G. Eelen, T.K. Karakach, H. Yang, J. Wang, L. Bolund, L. Lin, B. Thienpont, X. Li, D. Lambrechts, Y. Luo, P. Carmeliet, An integrated gene expression landscape profiling approach to identify Lung tumor endothelial cell heterogeneity and angiogenic candidates, Cancer Cell 37 (2020) 21–36, https://doi.org/10.1016/j.ccell.2019.12.001, e13.

[40] J.W. Williams, H. Winkels, C.P. Durant, K. Zaitsev, Y. Ghosheh, K. Ley, Single cell RNA sequencing in atherosclerosis research, Circ. Res. 126 (2020) 1112–1126, https://doi.org/10.1161/CIRCRESAHA.119.315940.

[41] S.W. Lukowski, J. Patel, S.B. Andersen, S.L. Sim, H.Y. Wong, J. Tay, I. Winkler, J. E. Powell, K. Khosrotehrani, Single-cell transcriptional profiling of aortic endothelium identifies a hierarchy from endovascular progenitors to differentiated cells, Cell Rep. 27 (2019) 2748–2758, https://doi.org/10.1016/j.celrep.2019.04.102, e3.